Nanoscale Advances

ROYAL SOCIETY OF CHEMISTRY

COMMUNICATION

View Article Online
View Journal | View Issue

Cite this: *Nanoscale Adv.*, 2021, **3**, 2217

Antiferromagnetic spin ordering in two-dimensional honeycomb lattice of SiP_3†

Souren Adhikary,[a] Sudipta Dutta *[ab] and Sasmita Mohakud*[ab]

Received 6th February 2021
Accepted 20th March 2021

DOI: 10.1039/d1na00101a

rsc.li/nanoscale-advances

Magnetism in low-dimensional materials has been of sustained interest due to its intriguing quantum mechanical origin and promising device applications. Here, we propose a buckled honeycomb lattice of stoichiometry SiP_3, a two-dimensional binary group-IV and V material that exhibits an antiferromagnetic ground state with itinerant electrons. Here we perform elemental Si substitution in pristine blue phosphorene to downshift the Fermi energy and induce the Fermi instability that results in a spin polarized ground state. Within first-principles calculations, we observe antiferromagnetic spin alignment between adjacent ferromagnetic triangular domains where each Si atom is coupled with three neighboring P atoms with a ferromagnetic interaction. Such unique spin structure and resulting magnetic ground state are unprecedented in defect-free two-dimensional materials made of only p-block elements. This metal-free magnetism can be exploited for advanced spintronic and memory storage applications.

1 Introduction

Two-dimensional (2D) materials have been of great interest in recent times, owing to their interesting electronic properties arising from quantum confinement.[1,2] Inspired by the isolation of graphene, a Dirac semimetal, extensive investigations have been continuing over the last decade to explore a plethora of other 2D materials with varying functionalities.[3,4] One of the major quests has been the magnetism in such reduced dimension, mainly owing to their application possibilities in advanced spintronic and memory devices.[5–7] This has so far been achieved by structural or chemical modifications, defect engineering, doping, external perturbations *etc.*[8–12]

In this regard, graphene nanoribbon has been one of the most extensively studied systems, where the zigzag edge tends to localize the spins.[13–15] Actually, the partial flat bands at Fermi energy in non-interacting approximation, originating from zigzag edges result in diverging density of states (DOS) and consequent Fermi instability. Inclusion of electron–electron interactions splits those degenerate bands at Fermi energy to open up a gap and localizes the spins in ferrimagnetic alignment along the zigzag edge.[2] These theoretical predictions have been confirmed within scanning tunneling spectroscopy experiments as well.[16–18] However, experimental realization of long and smooth zigzag edge has still been challenging.[19] The observation of such magnetic ordering has been elusive in defect-free 2D materials till the recent discovery of transition metal trichalcogenides, halides,[20] borides[21] and carbon organic frameworks.[22–24] It is mainly due to the fact that, the long range magnetic ordering gets suppressed due to thermal agitation, as described by Mermin–Wagner theory.[25]

However, the recent observations of pristine 2D ferromagnetic van der Waals crystals containing transition metal atoms have shown the influence of uniaxial magnetic anisotropy to stabilize such magnetic ordering of d-electrons.[20,26] This can be exploited for advanced device applications. However, the metal-based devices have several limitations, *e.g.*, high cost, heavy, low durability and susceptible to corrosion. Therefore, here we asked a question: can we design a metal-free 2D magnetic material ? This lead us to search for 2D materials that are made of p-block elements. Here, we report silicon (Si) substituted 2D blue phosphorene, SiP_3 which shows overall antiferromagnetic ground state with out-of-plane spin orientation. The magnetism has been achieved by inducing Fermi instability *via* downshifting the Fermi energy of nonmagnetic blue phosphorene by hole doping through elemental Si substitution.

2 Computational details

We adopt the density functional theory (DFT) as implemented in SIESTA[27] to explore the electronic and magnetic properties of

[a]*Department of Physics, Indian Institute of Science Education and Research (IISER) Tirupati, Tirupati - 517507, Andhra Pradesh, India. E-mail: sdutta@iisertirupati.ac.in; smohakud@gmail.com*

[b]*Center for Atomic, Molecular and Optical Sciences & Technologies, Indian Institute of Science Education and Research (IISER) Tirupati, Tirupati - 517507, Andhra Pradesh, India*

† Electronic supplementary information (ESI) available. See DOI: 10.1039/d1na00101a

pristine and doped 2D blue phosphorene. Generalized Gradient Approximation (GGA) is considered with Perdew–Burke–Ernzerhof (PBE) exchange and correlation functional.[28] Troullier Martin scheme is adopted to generate the norm-conserving pseudopotentials.[29] Double-ζ polarized basis set is used with 400 Ry energy cut-off for real space mesh size. Structural optimizations are performed using conjugate-gradient method along with the relaxation of lattice vectors until force on each atoms becomes less than 0.01 eV Å^{-1}. We consider a vacuum of 15 Å in the non-periodic direction to avoid any interaction between adjacent unit cells. We consider Brillouin zone sampling over 16 × 16 × 1 and 48 × 48 × 1 Monkhorst–Pack grids for geometric relaxation and subsequent electronic property calculations, respectively. To check the dynamical stability, we further investigate the phonon dispersions using 2 × 3 × 1 supercell and *k*-mesh of 16 × 16 × 1 with mesh cut-off of 1600 Ry. Since, the consideration of localized orbital basis in SIESTA overestimates the band gap, we perform further calculations using plane-wave basis as implemented in VASP[30–32] for comparison and present them in ESI.†

3 Results and discussion

The structure of 2D monolayer pristine blue phosphorene is shown in Fig. 1(a). It shows honeycomb lattice with out-of-plane buckling (Δ_z) and its ground state does not show any spin-polarization. This system has been obtained experimentally and is known to exhibit high charge carrier mobility.[33,34] In Fig. 1(b), we present the electronic band dispersion of its 2 × 2 supercell which shows semiconducting band gap of ∼2 eV. Most interestingly, the band structure shows nearly flat top of the valence band and corresponding diverging DOS. We have been motivated by the fact that, if the Fermi energy can be down-shifted by hole doping to align with this diverging DOS, it might be possible to achieve magnetic ground state, as observed in case of zigzag edge graphene nanoribbons.[13] However, since the Fermi energy can be located anywhere in the theoretically estimated large semiconducting gap of ∼2 eV, it is experimentally unlikely to achieve the required Fermi level shift by p-type doping through gate electrode. Therefore, we adopt the strategy of elemental substitution of phosphorus (P) atoms by silicon (Si) atoms that has one less electron, to dope the system with holes.

This kind of elemental substitution is known to produce shift in Fermi energy by a large extent, as has been observed in case of 2D binary compound BC_3.[35–37] This exhibits planar honeycomb lattice with homogeneously placed substitutional boron (B) atoms in graphene lattice, such that, every carbon hexagon is surrounded by six B atoms.[38,39] Owing to one less electron in each B atom as compared to carbon (C) atom, the system gets hole doped with consequent down-shift of Fermi energy by ∼2 eV.[36] Therefore, such elemental substitution appears to be a viable solution in present study as well and we consider similar stoichiometry of SiP_3 to bring the Fermi energy down. Fig. 1(c) shows the structure of SiP_3, where phosphorus hexagons are symmetrically surrounded by six Si atoms, resulting in a 8 atom unit cell. That is why, we choose to present the band structure of 2 × 2 supercell of pristine blue phosphorene as well in Fig. 1(b) for better comparison. Such group-IV–group-V binary compounds indeed exist in layered form with same stoichiometry and lattice geometry, as evident from previous studies.[40–44]

We investigate the substitution by other group-IV elements, *e.g.*, C, Ge and Sn as well. However, we observe minimal structural distortion in case of Si substitution in pristine blue phosphorene (see Tables S1 and S2 in ESI†). This can be attributed to the minimal difference of atomic radius of P and Si for being in the same period and hence unaltered hybridization as compared to pristine blue phosphorene and silicene (see Table S3 in ESI†). In Table 1, we present the structural parameters of pristine and Si substituted blue phosphorene, which show close resemblance. However, due to the change in the buckling parameter for P–Si bond the associated ∠P–P–Si (θ_2) show considerable increase (see Table 1 and Fig. 1(c)).

For further stability analysis, we investigate the phonon dispersion of SiP_3 and present in Fig. 2. The absence of any imaginary phonon mode and well separated acoustic and optical modes clearly indicate the dynamical stability of the system. The quadratic dispersion of the flexural out-of-plane (ZA) acoustic mode shows nice resemblance with that of pristine blue phosphorene,[45] showing the robust and rigid 2D architecture. Moreover, the in-plane elastic response shows

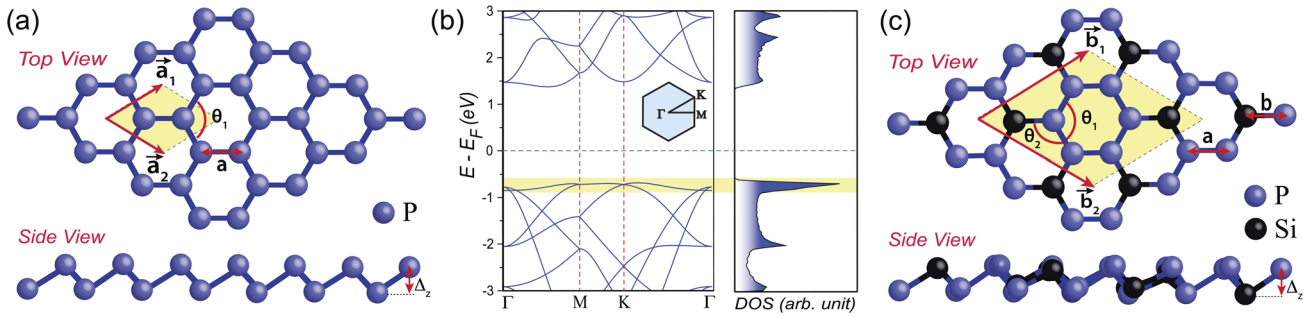

Fig. 1 (a) The structure of pristine blue phosphorene, (b) band structure and density of states (DOS) of the same in 2 × 2 supercell and (c) the structure of SiP_3. The shaded rhombuses in (a) and (c) show the corresponding unit cells with lattice vectors, $\overrightarrow{a_{1/2}}$ and $\overrightarrow{b_{1/2}}$, respectively. The P–P (P–Si) bond length is denoted by a (b) and the ∠P–P–P (∠P–P–Si) is denoted by θ_1 (θ_2). Δ_z quantifies the out-of-plane buckling. The vertical and horizontal dashed lines in (b) show high-symmetric points in the irreducible Brillouin zone, shown in the inset and Fermi energy, respectively.

Table 1 The structural parameters of pristine blue phosphorene and SiP_3: lattice constants (a_1/b_1), P–P bond lengths (a), P–Si bond lengths (b), ∠P–P–P (θ_1), ∠P–P–Si (θ_2) and out-of-plane buckling parameters ($\Delta_{z(P-P)}$ and $\Delta_{z(P-Si)}$). All these are shown in Fig. 1(a) and (c). Note that, the lengths and angles are in Å and degree, respectively

System	a_1/b_1	$a(b)$	θ_1	θ_2	$\Delta_{z(P-P)}$	$\Delta_{z(P-Si)}$
Phosphorene	3.326	2.31 (—)	92.22	—	1.28	—
SiP_3	6.926	2.30 (2.31)	91.78	97.92	1.287	0.983

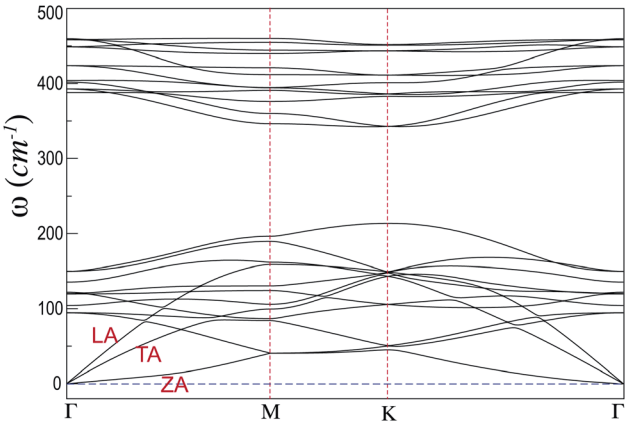

Fig. 2 Phonon dispersion of SiP_3 system with high-symmetric points (vertical dashed lines).

isotropic nature, as evident from the similar slopes of longitudinal acoustic branch (LA) near Γ points at both the ends of Fig. 2. This observation also resembles with that of pristine blue phosphorene[45] and proves the existence of the inversion symmetry even with asymmetric P–P and P–Si buckling amplitudes in SiP_3.

We then calculate the electronic band structure and density of states of SiP_3 without and with spin-polarization. The band structure for nonmagnetic (NM) approximation shows partial dispersion-less band and corresponding diverging density of states near the Fermi energy (see Fig. 3(a)). These bands originate from considerable band mixing due to strong hybridization of P and Si. This is confirmed by further fat band calculation that shows complete hybrid nature of the bands near Fermi energy, with contributions from 3p orbitals of both P and Si. Nevertheless, the Fermi instability is still arising from the dispersion-less hybrid bands that can potentially lead to magnetic ground state, as has been observed in case of zigzag edge graphene nanoribbons.[2,13–18]

Further spin-polarized calculations with both ferromagnetic (FM) and antiferromagnetic (AFM) initial guesses with subsequent self-consistent electronic relaxations show 13 and 74 meV per unit cell more stability as compared to the NM state, respectively. This clearly indicates the preferential magnetic ground state with non-zero spin moments on atomic sites in 2D SiP_3. This observation is in striking contrast to that of other known 2D materials made of p-block elements, which do not allow any bulk polarization of spins in absence of any defects,

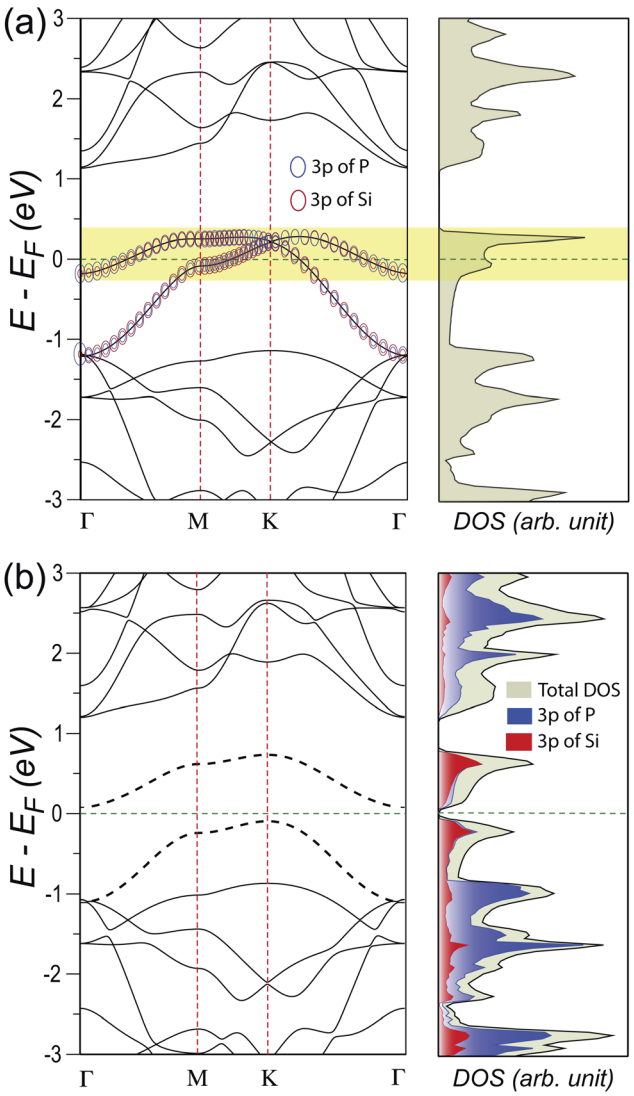

Fig. 3 (a) The band structure and the density of states (DOS) of SiP_3 system in nonmagnetic ground states. The contributions from 3p orbitals of Si and P atoms are shown in terms of fat bands for the two bands near Fermi energy. The size of the circles is proportional to the extent of contribution. (b) The band structure and DOS of the same system in antiferromagnetic ground state. The two central bands are shown as dotted lines. The projected DOS from 3p orbitals of Si and P are also shown. The vertical (horizontal) lines show the high-symmetric points (Fermi energy).

e.g., vacancies or edges.[2,8] Such unique magnetic ground state of 2D SiP_3 has not been observed in case of other group-IV elemental substitutions as well,[42–44] due to the lack of Fermi instability in their NM energy dispersions (see Fig. S1 in ESI†). Owing to the highest stability, we further proceed with the AFM ground state of SiP_3.

We first investigate the stabilization energy of such ground state as compared to that of pristine one. The stabilization energies per atom are calculated using the equation, $E_{\text{stability}} = \left(E_{\text{total}} - \sum_i N_i E_i\right) \Big/ N$. Here E_{total} is the total energy of the system, E_i and N_i are the single atom energy and total

number of atoms of i-th element and N is the total number of atoms in the unit cell. We find the SiP_3 system is more stable than the pristine blue phosphorene by ~0.11 eV per atom. Even the system with stoichiometry $Si_{0.5}P_{3.5}$, *i.e.*, with only one substituted Si atom in the 2 × 2 supercell of blue phosphorene shows a ~0.04 eV per atom higher stability as compared to its parent system. This indicates a stability gain by gradual Si replacement in pristine layer even at room temperature (~25 meV). Such stability analysis along with the stable phonon dispersion shows that the synthesis of SiP_3 system is experimentally conducive. It can be achieved by selective and systematic Si replacement in blue phosphorene, as has been observed in recent experiments.[46–49]

Now in the AFM ground state, the two NM hybrid bands at Fermi energy gets separated and opens up a tiny indirect band gap of 0.17 eV, as can be seen in Fig. 3(b). The hybrid nature of these two bands is evident from the comparable projected DOS from 3p orbitals of both P and Si. Such a small gap can easily be closed by thermal fluctuation of the Fermi surface at finite temperature or by small external perturbations. Our further investigation within plane-wave approximation results in comparatively more dispersive bands that cross the Fermi energy and results in metallic behavior (see Fig. S2 in ESI†). Therefore, we infer the ground state of SiP_3 to be more likely an itinerant AFM state. In addition to that, it shows very peculiar spin ordering. The spins on each Si atom and its three neighboring P atoms are ferromagnetically coupled. However, the hexagons consisting of only P atoms show perfectly bipartite nature of opposite spin alignments between nearest neighbors. This leads to two triangular tiny ferromagnetic domains with opposite spin orientations in the rhombus unit cell, as can be seen in Fig. 4(a). The AFM ground state ensures localization of opposite spins on two Si atoms in the unit cell. Further charge transfer from neighboring P atoms to the Si atom creates imbalance between up and down spins on each P atom, resulting in a bipartite spin ordering in the P-hexagon (see Table S3 in ESI†). Such charge transfer happens due to the Lewis base character of P atoms. This sets up the ferromagnetic coupling between neighboring P and Si atoms, leading to the overall AFM spin ordering in SiP_3, as shown schematically in Fig. 4(b). Note that, such Fermi instability induced long range magnetic ordering has been observed in case of zigzag edge graphene nanoribbons.[2,13–18]

Our detailed investigation of systems with other group IV elements, *e.g.*, C, Ge and Sn always result in NM ground state within both localized and plane-wave basis (see Tables S4, S5 and Fig. S1, S3 in ESI†).

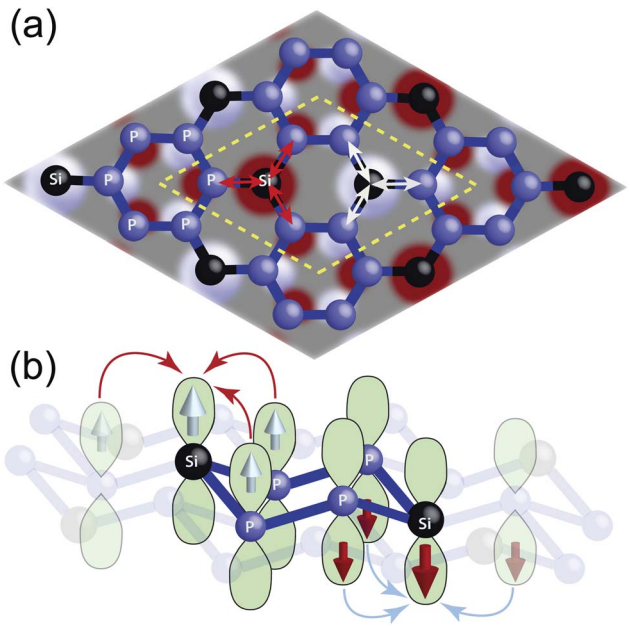

Fig. 4 (a) Spin–density plot of SiP_3 with two different colors denoting up and down spin orientations. The dashed rhombus shows the unit cell and the double-headed arrows show the ferromagnetic coupling. (b) Schematic representation of π-electron orbitals of SiP_3 with spin transfer directions shown by the arrows.

4 Conclusions

In conclusion, within first-principles calculations, we exploit the partially flat top of the valence band and consequent diverging density of states of pristine blue phosphorene to induce Fermi instability. This has been done by downshift of Fermi energy *via* elemental Si substitution that leads to SiP_3 stoichiometry. This system exhibits itinerant AFM ground state with a unique spin ordering, where each Si atom is ferromagnetically coupled with three neighboring P atoms, however maintaining antiferromagnetic spin orientation between such neighboring triangular domains. This unique spin alignment primarily arises due to the charge transfer from neighboring P atoms to Si atoms. The *ab initio* energetics and phonon dispersion analysis show stability of this proposed system in ambient conditions. The observation of such magnetic ground state is unprecedented in 2D materials that are made of purely p-block elements in absence of any defect, twist or external perturbations. Further experimental exploration is necessary to confirm such long range ordering at finite temperature. This metal-free magnetism with unique spin texture can find huge spintronic, memory storage and qubit applications and will tempt further theoretical and experimental explorations.

Author contributions

SD and SM have defined the project. SA has performed the calculations. All the authors have analyzed the results and written the manuscript.

Conflicts of interest

The authors declare no competing financial interest.

Acknowledgements

SA and SD thank IISER Tirupati for Intramural Funding and Science and Engineering Research Board (SERB), Dept. of Science and Technology (DST), Govt. of India for Early Career

Research (ECR) award grant (ECR/2016/000283). SM acknowledges the SERB, DST, Govt. of India for ECR award grant (ECR/2016/001431) and DST INSPIRE-Faculty award grant (IFA 14-PH-96). The authors thank Prof. K. Wakabayashi (Kwansei Gakuin University) for illuminating discussions. The support and the resources provided by 'PARAM Brahma Facility' under the National Supercomputing Mission, Government of India at the Indian Institute of Science Education and Research (IISER) Pune are gratefully acknowledged.

Notes and references

1 A. H. Castro Neto, F. Guinea, N. M. R. Peres, K. S. Novoselov and A. K. Geim, *Rev. Mod. Phys.*, 2009, **81**, 109.
2 K. Wakabayashi and S. Dutta, *Solid State Commun.*, 2012, **152**, 1420.
3 K. S. Novoselov, A. Mishchenko, A. Carvalho and A. H. Castro Neto, *Science*, 2016, **353**, 6298.
4 A. K. Geim and K. S. Novoselov, *Nat. Mater.*, 2007, **6**, 183.
5 K. Wakabayashi, M. Fujita, H. Ajiki and M. Sigrist, *Phys. Rev. B: Condens. Matter Mater. Phys.*, 1999, **59**, 8271.
6 W. Han, R. K. Kawakami, M. Gmitra and J. Fabian, *Nat. Nanotechnol.*, 2014, **9**, 794.
7 A. Avsar, H. Ochoa, F. Guinea, B. Özyilmaz, B. J. van Wees and I. J. Vera-Marun, *Rev. Mod. Phys.*, 2020, **92**, 021003.
8 O. V. Yazyev and L. Helm, *Phys. Rev. B: Condens. Matter Mater. Phys.*, 2007, **75**, 125408.
9 Y. W. Son, M. L. Cohen and S. G. Louie, *Nature*, 2006, **444**, 347.
10 S. Dutta, A. K. Manna and S. K. Pati, *Phys. Rev. Lett.*, 2009, **102**, 096601.
11 A. L. Sharpe, E. J. Fox, A. W. Barnard, J. Finney, K. Watanabe, T. Taniguchi, M. A. Kastner and D. Goldhaber-Gordon, *Science*, 2019, **365**, 605.
12 T. M. R. Wolf, J. L. Lado, G. Blatter and O. Zilberberg, *Phys. Rev. Lett.*, 2019, **123**, 096802.
13 M. Fujita, K. Wakabayashi, K. Nakada and K. Kusakabe, *J. Phys. Soc. Jpn.*, 1996, **65**, 1920.
14 K. Wakabayashi, M. Sigrist and M. Fujita, *J. Phys. Soc. Jpn.*, 1998, **67**, 2089.
15 A. Yamashiro, Y. Shimoi, K. Harigaya and K. Wakabayashi, *Phys. Rev. B: Condens. Matter Mater. Phys.*, 2003, **68**, 193410.
16 C. Tao, *et al.*, *Nat. Phys.*, 2011, **7**, 616.
17 G. Z. Magda, X. Jin, I. Hagymási, P. Vancsó, Z. Osváth, P. Nemes-Incze, C. Hwang, L. P. Biro and L. Tapaszto, *Nature*, 2014, **514**, 608.
18 S. Wang, L. Talirz, C. A. Pignedoli, X. Feng, K. Müllen, R. Fasel and P. Ruffieux, *Nat. Commun.*, 2016, **7**, 11507.
19 P. Ruffieux, *et al.*, *Nature*, 2016, **531**, 489.
20 C. Gong and X. Zhang, *Science*, 2019, **363**, eaav4450.
21 C. Tang, K. Ostrikov, S. Sanvito and A. Du, *Nanoscale Horiz.*, 2021, **6**, 43.
22 E. Jin, *et al.*, *Science*, 2017, **357**, 673.
23 W. Jiang, H. Huang and F. Liu, *Nat. Commun.*, 2019, **10**, 2207.
24 Y. Zhou and F. Liu, *Nano Lett.*, 2021, **21**, 230.
25 N. D. Mermin and H. Wagner, *Phys. Rev. Lett.*, 1966, **17**, 1133.
26 J. L Lado and J. Fernández-Rossier, *2D Mater.*, 2017, **4**, 035002.
27 J. M Soler, E. Artacho, J. D Gale, A. García, J. Junquera, P. Ordejón and D. Sánchez-Portal, *J. Phys.: Condens. Matter*, 2002, **14**, 2745.
28 J. P. Perdew, K. Burke and M. Ernzerhof, *Phys. Rev. Lett.*, 1996, **77**, 3865.
29 N. Troullier and J. L. Martins, *Phys. Rev. B: Condens. Matter Mater. Phys.*, 1991, **43**, 1993.
30 G. Kresse and J. Furthmüller, *Phys. Rev. B: Condens. Matter Mater. Phys.*, 1996, **54**, 11169.
31 G. Kresse and J. Furthmüller, *Comput. Mater. Sci.*, 1996, **6**, 15.
32 G. Kresse and D. Joubert, *Phys. Rev. B: Condens. Matter Mater. Phys.*, 1999, **59**, 1758.
33 J. L. Zhang, S. Zhao, C. Han, Z. Wang, S. Zhong, S. Sun, R. Guo, X. Zhou, C. D. Gu, K. D. Yuan, Z. Li and W. Chen, *Nano Lett.*, 2016, **16**, 4903.
34 J. Zeng, P. Cui and Z. Zhang, *Phys. Rev. Lett.*, 2017, **118**, 046101.
35 D. Tománek, R. M. Wentzcovitch, S. G. Louie and M. L. Cohen, *Phys. Rev. B: Condens. Matter Mater. Phys.*, 1998, **37**, 3134(R).
36 S. Dutta and K. Wakabayashi, *J. Mater. Chem.*, 2012, **22**, 20881.
37 T. Kameda, F. Liu, S. Dutta and K. Wakabayashi, *Phys. Rev. B: Condens. Matter Mater. Phys.*, 2019, **99**, 075426.
38 H. Tanaka, Y. Kawamata, H. Simizu, T. Fujita, H. Yanagisawa, S. Otani and C. Oshima, *Solid State Commun.*, 2005, **136**, 22.
39 H. Yanagisawa, T. Tanaka, Y. Ishida, E. Rokuta, S. Otani and C. Oshima, *Phys. Rev. B: Condens. Matter Mater. Phys.*, 2006, **73**, 045412.
40 P. C. Donohue and H. S. Young, *J. Solid State Chem.*, 1970, **1**, 143.
41 J. Gullman and O. Olofsson, *J. Solid State Chem.*, 1972, **5**, 441.
42 B. Ghosh, S. Puri, A. Agarwal and S. Bhowmick, *J. Phys. Chem. C*, 2018, **122**, 18185.
43 Y. Jing, Y. Ma, Y. Li and T. Heine, *Nano Lett.*, 2017, **17**, 1833.
44 M. Kar, R. Sarkar, S. Pal and P. Sarkar, *Phys. Rev. B: Condens. Matter Mater. Phys.*, 2020, **101**, 195305.
45 Z. Zhu and D. Tománek, *Phys. Rev. Lett.*, 2014, **112**, 176802.
46 H. Wang, *et al.*, *Nano Lett.*, 2012, **12**, 141.
47 M. Tripathi, A. Mittelberger, N. A. Pike, C. Mangler, J. C. Meyer, M. J. Verstraete, J. Kotakoski and T. Susi, *Nano Lett.*, 2018, **18**, 5319.
48 S.-Y. Cho, H.-J. Koh, H.-W. Yoo and H.-T. Jung, *Chem. Mater.*, 2017, **29**, 7197.
49 K. Zhang, *et al.*, *Nano Lett.*, 2015, **15**, 6586.